THE JOURNAL OF PHYSICAL CHEMISTRY B
A JOURNAL OF THE AMERICAN CHEMICAL SOCIETY

pubs.acs.org/JPCB Article

# Bulk versus Interface Nucleation of $CO_2$ Hydrates from Computer Simulations

Joanna Grabowska,* Samuel Blazquez, Carlos Vega, and Eduardo Sanz*

Cite This: https://doi.org/10.1021/acs.jpcb.5c07607 Read Online

ACCESS | Metrics & More | Article Recommendations | Supporting Information

**ABSTRACT:** Gas hydrates are of great relevance to both the oil industry and the environment. Understanding how these solid structures nucleate from aqueous solutions is essential for controlling their formation. Experimental studies have often suggested that hydrate nucleation originates at the interface between the aqueous phase and the guest-molecule reservoir. To assess this hypothesis, we perform molecular dynamics simulations of $CO_2$ hydrate nucleation. First, we place hydrate seeds at different positions relative to the interface and monitor their evolution, finding that seeds embedded in the bulk are more likely to grow than those located near or at the interface. Second, we analyze spontaneous nucleation simulations with and without an interface. Our previous work showed that nucleation rates are indistinguishable in both systems, strongly indicating that the interface does not play a role. Here, trajectory analysis reveals that hydrates nucleate in regions of locally high $CO_2$ concentration, which arise spontaneously in the bulk and are not associated with the interface. Our results indicate that hydrate nucleation does not preferentially occur at the interface, at least under the deep supercooling conditions explored in this work. Further work at higher temperatures, and considering alternative nucleation locations, is needed to reconcile experiments and simulations, and thereby reach a deep understanding of the mechanism of hydrate formation.

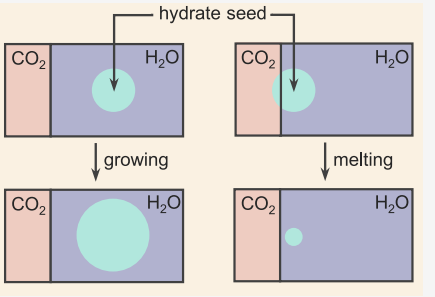




## 1. INTRODUCTION

Clathrate hydrates are crystalline structures in which gas molecules are trapped within cages of water molecules.[1] Methane hydrates are primarily found in deep-sea sediments and permafrost regions, and serve as a substantial reservoir of methane and other fuel molecules. In addition to their potential as an energy source, gas hydrates offer a promising avenue for carbon dioxide ($CO_2$) sequestration, as $CO_2$ could replace methane within hydrate structures,[2−5] providing a dual benefit of reducing greenhouse gas emissions while facilitating methane extraction. Hydrogen hydrates are also important because they offer a potential method for safe and compact storage of hydrogen, supporting the transition to cleaner energy sources. Methane hydrates, however, pose significant challenges for the oil and gas industry, particularly due to their tendency to form blockages in pipelines during hydrocarbon production and transportation, leading to operational inefficiencies and safety risks.[6] It is thereby crucial to characterize and understand the formation and stability of hydrates.

Numerous experimental studies[7−15] have been conducted to better understand the formation, growth and dissociation of gas hydrates under various thermodynamic and kinetic conditions. Researchers have investigated the effects of temperature, pressure, gas composition and the presence of inhibitors or promoters on hydrate crystallization and stability.

There seems to be compelling experimental evidence that hydrates nucleate at the interface between the solution and the hydrate former reservoir.[1,16−21] This is a likely scenario given that the solubility of hydrate former molecules ($CO_2$, $CH_4$, $H_2S$ etc.) in water is typically much lower than the proportion of gas former molecules in the solid hydrate, which is 1 molecule per 5.75 water molecules in a perfect sI hydrate lattice. Thus, it appears reasonable that only in the vicinity of the interface there is enough hydrate former concentration to nucleate the hydrate. Experimental techniques, however, do not enable a direct visualization of the first hydrate embryo that nucleates from a disordered molecular arrangement, given its nanoscopic size and its short lifespan.

A theoretical approach is very useful for understanding and rationalizing the competition between homogeneous and interfacial nucleation; however, the values of the relevant parameters that enter the theoretical description require experimental validation, and the theory does not provide a molecular-level representation of the nucleation process.[22] Molecular simulations can help bridge the gap in our understanding of nucleation at a molecular scale,[23−48] particularly so with the emergence of realistic water models

Received: November 6, 2025
Revised: March 13, 2026
Accepted: March 13, 2026

that have proven to be highly accurate in predicting the equilibrium behavior of real hydrates.[49−53] Most simulation studies of hydrate nucleation, however, focus on the homogeneous nucleation of the hydrate in the bulk aqueous solution[27,30,31,34,38,39,54−56] (in many cases with a guest molecule concentration way higher than the saturation concentration to enhance the nucleation rate) and the hypothetical location of the nucleus at the interface has not been properly assessed.

Some clues regarding the location of hydrate nucleation can be found in refs 57 and 58. In ref 57, focused on unveiling the molecular path leading to the formation of hydrates (blobs of guest molecules give rise to hydrate nuclei), it was mentioned that nuclei can indistinctly appear in the bulk or at the interface. According to ref 58, in contrast, nucleation in the bulk is not considered as a possibility (it either takes place at the interface with the hydrate-former rich phase or with a solid substrate at low and high temperatures respectively).

The fact that homogeneous nucleation cannot compete with nucleation at the interface is inconsistent with our recent simulation study.[55] In ref 55 we conducted simulations of spontaneous $CO_2$ hydrate nucleation from a bulk $CO_2$ saturated solution and from a $CO_2$ saturated solution in contact with a $CO_2$ reservoir through a flat interface. The frequency of hydrate nucleation was the same in both cases, suggesting that the interface does not promote nucleation, at least under the studied conditions (245 and 250 K, 400 bar).

In this work, we use Molecular Dynamics (MD) simulations to clarify whether hydrates preferentially appear at the solution-hydrate former interface. More specifically, we place $CO_2$ hydrate seeds at different locations relative to the $CO_2$-solution interface and track their evolution in constant pressure, constant temperature (NpT) MD simulations. We find that, in the conditions of our study (400 bar and 255 K), proximity to the interface hinders the growth of $CO_2$ hydrate seeds, leading to faster nucleation rates in the bulk than at the interface.

Our work highlights that hydrate nucleation in the bulk aqueous solution is faster than at the interface with the hydrate former. This result seems to be at odds with the general understanding that nucleation is faster at the interface.[1,16−21] A study at higher temperatures (closer to the dissociation temperature, where experiments are typically carried out) is needed to explore the possibility of a crossover of nucleation location along temperature. Also, nucleation at the container walls or assisted by impurities are possibilities that could reconcile our results with the widely visualized observation of the appearance of hydrates at the interface in experimental research.

## 2. METHODOLOGY

### 2.1. Simulation Details

Water and $CO_2$ molecules are modeled with TIP4P/Ice[59] and TraPPE,[60] respectively. Water−$CO_2$ dispersive interactions are treated with the modified Lorentz−Berthelot rule proposed by Míguez et al. (which simply consists of multiplying by 1.13 the cross energy parameter given by Lorentz−Berthelot).[50] These potentials yield accurate predictions of the $CO_2$ hydrate three-phase line, with the dissociation temperature $T_3$ at 400 bar matching the experimental value (286 K in experiment versus 290 K in simulations).[61] The model, however, is not perfect. For instance, it overestimates the solubility of $CO_2$ in liquid water at low temperatures.[62] Importantly, while this force-field limitation affects the absolute value of the $CO_2$ solubility, it does not alter the qualitative conclusions of the present work. All simulations were performed using the same force field, and comparisons between bulk and interfacial nucleation were therefore made under internally consistent conditions.

We focus on a pressure of 400 bar and most simulations are carried out at 255 K (i.e., 35 K supercooling). We focused on a pressure value typical of experiments in order to make predictions at experimentally relevant conditions and to enhance the solubility of $CO_2$ in water. Other pressure values should be investigated to properly assess the role of this variable, that may affect the nucleation rate and pathway.[22]

MD simulations were used to obtain all the results presented in this work. The simulations were conducted with the use of the GROMACS package.[63,64] The leapfrog algorithm with a time step of 2 fs has been used to integrate the equations of motion. Temperature was kept constant with the use of a Nosé−Hoover[65,66] thermostat with a relaxation time of 2 ps, while pressure was kept constant with the Parrinello−Rahman[67] barostat with the same relaxation time. The isothermal−isobaric ensemble ($Np_xT$) has been used for most of the runs (with the barostat applied only along the $x$ direction, which is normal to the interface); in some cases, NVT simulations were employed (details of the specific simulations will be provided below). For dispersive and Coulombic interactions, a cutoff of 1 nm has been used. Particle Mesh Ewald method[68] has been used to compute electrostatic interactions. Long-range corrections for dispersive interactions were not used in our simulations.

All simulation systems were prepared using a two-phase system, where an aqueous solution of $CO_2$ molecules was in contact - via a planar interface - with a $CO_2$ reservoir. The size of this system was $11.6 \times 8.5 \times 8.5$ nm$^3$, where the $x$ direction is perpendicular to the interface, and it contained 15735 molecules of water and 5 896 molecules of $CO_2$.

The initial configuration of the two-phase system was prepared by combining pre-equilibrated simulation boxes of pure $CO_2$ and of a $CO_2$ aqueous solution (with $CO_2$ molar fraction of 0.085, which is close to the expected equilibrium solubility of $CO_2$ in water for the selected model under the studied conditions).[61] The obtained system was then equilibrated for 40 ns at 255 K and 400 bar, in an anisotropic $Np_xT$ ensemble (i.e., the pressure was allowed to fluctuate only in the direction perpendicular to the interface). During the equilibration run, we monitored changes of the molar fraction of $CO_2$ in the aqueous phase, which reached a stable value of approximately 0.077 after 20 ns. The equilibration run was continued for another 20 ns to ensure that the $CO_2$ concentration in the aqueous phase remained at equilibrium.

After equilibration of the aqueous solution in contact with the $CO_2$ reservoir, the Seeding method was used: $CO_2$ hydrate crystal seeds of varying sizes were extracted from a bulk sI hydrate crystal in which all cages were fully occupied by $CO_2$ molecules (the $CO_2$ hydrate was equilibrated beforehand at 255 K and 400 bar for 10 ns) and inserted into the prepared two-phase system. After this step, the interface between the inserted cluster and the surrounding fluid was equilibrated with the use of three different protocols as explained in Supporting Information.

For all equilibration protocols, 6 types of systems were prepared, differing in the positioning of the seed with respect to the $CO_2$-aqueous solution interface. The different seed


https://doi.org/10.1021/acs.jpcb.5c07607
J. Phys. Chem. B XXXX, XXX, XXX−XXX

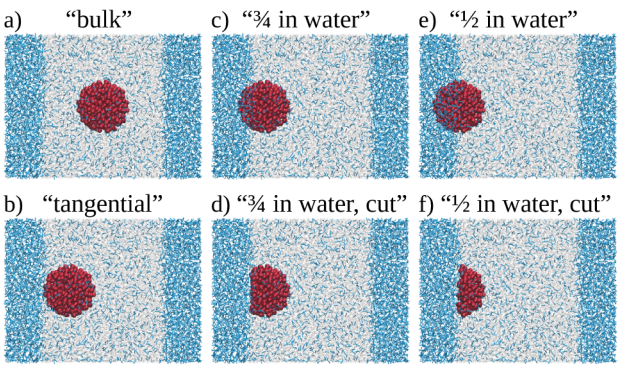


**Figure 1.** Snapshots of the seed locations and shapes investigated in this work: a) bulk, b) tangential, c) 3/4 in water, d) 3/4 in water, cut, e) 1/2 in water, f) 1/2 in water, cut. The color scheme of the figure is as follows: all molecules in the seed are represented as red spheres, water molecules and $CO_2$ molecules which do not belong to the seed are represented as gray and cyan sticks, respectively. The seeds presented in the figure have a radius equal to 1.5 nm. The graphic was created using VMD[69] software.

locations are shown in the snapshots in Figure 1. Below, we indicate how we refer to each of these locations and briefly describe them:

1. *Bulk* (Figure 1a): the seed is inserted in the middle of the aqueous phase, which is the type of setup we used in our previous Seeding work.[55]
2. *Tangential* (Figure 1b): the seed is inserted tangentially touching the $CO_2$-aqueous solution interface.
3. *3/4 in water* (Figure 1c): 1/4th of the seed diameter is immersed in the $CO_2$ liquid and the remaining 3/4th is immersed in the aqueous solution.
4. *3/4 in water, cut* (Figure 1d): same as *3/4 in water* but the part of the seed immersed in the $CO_2$ phase is cut off.
5. *1/2 in water* (Figure 1e): half of the seed is immersed in the $CO_2$ phase and the other half in the aqueous solution.
6. *1/2 in water, cut* (Figure 1f): same as *1/2 in water* but the part of the seed immersed in the $CO_2$ phase is cut off.

After the equilibration period we either fix the positions of atoms in the seed and let the seed grow or calculate the probability with which the unrestrained seed grows or shrinks. We determined the starting seed size as an average within the first 3 ns of a given production run.

To make sure that the *bulk* placement really corresponds to a molecular environment typical of a bulk aqueous solution we compute density profiles of $CO_2$ and water across the interface. Such density profiles, shown in Figure 2, enable a microscopic identification of the interface based on the spatial variation of water and $CO_2$ densities. As shown in the figure, deviations of the $CO_2$ concentration in the aqueous phase from its bulk value are confined to a region extending approximately 0.7−0.8 nm from the $CO_2$-rich phase. Beyond this distance, both the water density and the $CO_2$ concentration reach plateau values characteristic of bulk aqueous solution. Based on this analysis, we defined the interfacial region as the zone in which the density and composition vary continuously between the $CO_2$-rich and aqueous phases, and the bulk aqueous region as the region where these properties are spatially uniform. The hydrate seeds placed in the *bulk* configuration were positioned at distances greater than the extent of the influence of the interface on $CO_2$ concentration (see the dashed circle in Figure 2). At these distances, the local environment is indistinguishable from bulk water in terms of density and $CO_2$ concentration. Therefore, the hydrate seeds in systems labeled as *bulk* were not influenced by interfacial perturbations, while seeds placed closer to the $CO_2$-rich phase clearly reside within the interfacial region.

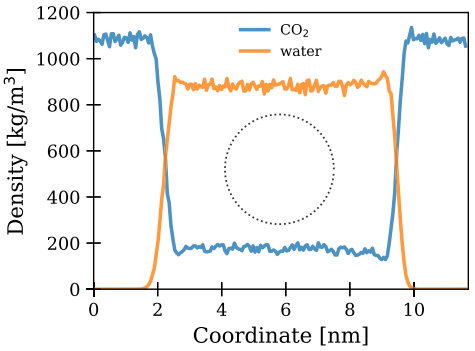


**Figure 2.** Density profiles of $CO_2$ and water along the direction perpendicular to the $CO_2$-water interface in the system used for seeding nucleation simulations. The circle marks the approximate spatial extent of the inserted hydrate seed of a radius of 1.7 nm and is included to provide a reference length scale relative to the profile gradients.

It is important to note that there is a substantial disparity between the $CO_2$ concentration in the aqueous phase under the conditions studied (molar fraction ≈ 0.077) and the $CO_2$ content in the hydrate phase (molar fraction ≈ 0.15). Under such conditions, the growth of hydrate-like structures could, in principle, lead to local $CO_2$ depletion, potentially decelerating further growth unless rapid replenishment from a nearby $CO_2$-rich phase occurs. In the present work, however, we focus on the nucleation regime and on the very early stages of critical nucleus growth. Within the time scales and cluster sizes probed by our seeding simulations, the $CO_2$ concentration in the aqueous phase remains effectively constant. The inserted seeds do not grow large enough to induce measurable $CO_2$ depletion in the surrounding solution, and consequently, mass transport limitations do not significantly influence the nucleation kinetics reported here.

## 3. RESULTS

### 3.1. Simulations with Hydrate Seeds in Fixed Positions

As described in the Methods section, we used six types of systems in our study, which differed in the position and/or the shape of the inserted hydrate seed. To investigate the growth behavior of the inserted seeds we fixed the positions of all their constituent atoms during the simulations (performed at 255 K and 400 bar). As a result, seed growth was observed in all runs, regardless of their placement. Figure 3 shows the configurations from one of the runs for each type of seed placement, at 0, 20, and 40 ns. The main conclusion is that seeds with an initially spherical shape maintained an approximately spherical form, whereas seeds prepared as truncated spheres at the beginning of the run tended to acquire a spherical shape during the simulation. The tendency of the seeds to acquire a


https://doi.org/10.1021/acs.jpcb.5c07607
J. Phys. Chem. B XXXX, XXX, XXX−XXX

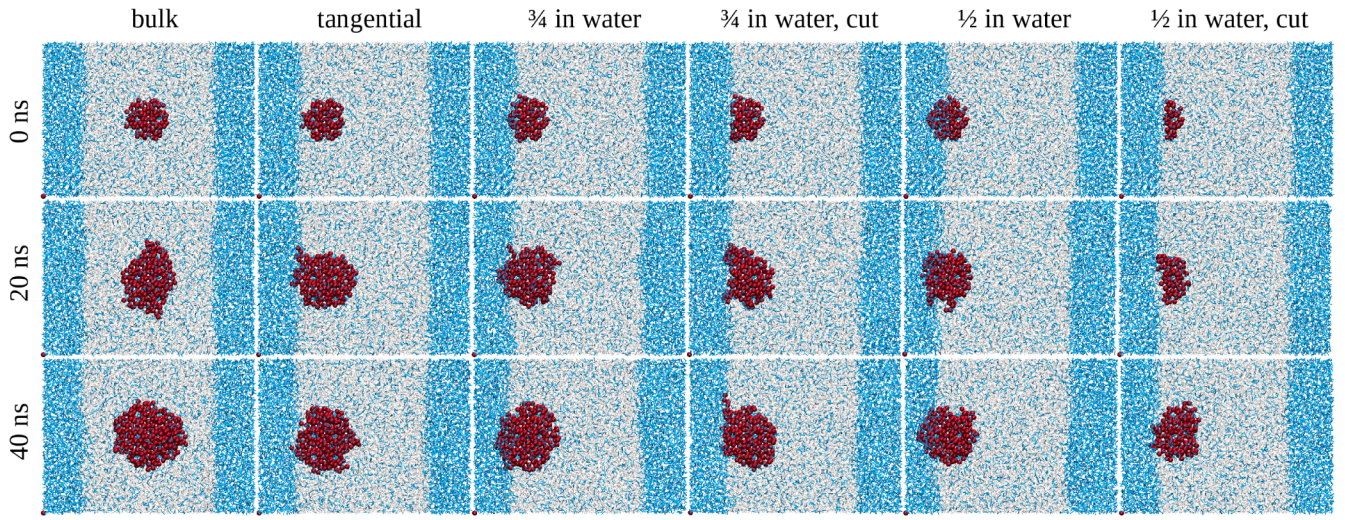


**Figure 3.** Configurations of the systems during the seeding simulations in which all molecules in the inserted hydrate seed were kept in fixed positions. Columns correspond to different types of seed locations whereas rows correspond to different times as indicated in the figure. Water molecules that were labeled as hydrate using a linear combination of $\overline{q}_3$ and $\overline{q}_{12}$ order parameter are presented as red spheres. Molecules of water in the liquid phase and molecules of $CO_2$ are shown as gray and cyan lines, respectively. It can be observed that the seeds retain a roughly spherical shape during the simulations and those which were originally only a part of a sphere recover the spherical shape as the simulations progress. The growth of the seeds occurs mainly toward the liquid phase; in some cases, a shift of the position of the interface can be observed in order to accommodate the growth. Keep in mind that during these simulations no melting of the seeds is possible, since the molecules of the original seed inserted into the systems are kept in fixed positions during the simulations. The graphic was created using VMD[69] software.

spherical shape suggests that the scenario of cap-shaped seeds nucleating on top of the $CO_2$-aqueous solution interface[22] does not accurately represent hydrate nucleation.

In Figure 4 the number of water molecules in the hydrate seed is plotted versus time for the different seed placements

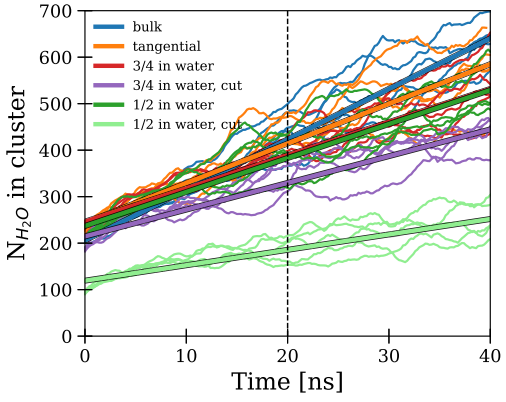


**Figure 4.** Changes of size of the hydrate seed during the seeding simulations in which all molecules in the inserted seed were kept in fixed positions. The radius of the seeds cut from the bulk hydrate was equal to 1.3 nm. Regression lines are included to show differences in the rates of growth of the seeds. The values of the slopes are (in 1/ns unit): 10.86 for *bulk*, 8.53 for *tangential*, 7.14 for *3/4 in water*, 5.75 for *3/4 in water, cut*, 7.30 for *1/2 in water* and 3.32 for *1/2 in water, cut*, respectively. The configurations obtained after 20 ns of simulation (indicated in the figure as a black dashed line) were used for the production runs (EQ3 equilibration protocol, described in Supporting Information).

under study. In order to quantify the seed size we count the number of molecules of water it contains using a linear combination of $\overline{q}_3$ and $\overline{q}_{12}$ order parameters, as we also did in our previous work.[55]

The starting radius of all seeds was equal to 1.3 nm. Consequently, the starting size of the seed, measured as the number of water molecules it contains, is smaller in the systems where a portion of the sphere was cut off. The growth rate can be quantified through the slope of a linear fit to the $N_{H_2O}(t)$ curves. Such linear fits are shown with thick lines in Figure 4 and the specific values of the slopes are included in the caption of the figure. The growth was, on average, faster for the *bulk* and *tangential* seed placements. For the seed placements where the nucleus is partially immersed in the $CO_2$-rich phase, *3/4 in water* and *1/2 in water*, the growth rate was a little slower, which indicates that the proximity of the interface decelerates the growth of the nucleus. The slowing down of the growth is even more pronounced for the systems where the seed was partially cut, although in these cases the comparison is not totally fair because the initial seed size is smaller. Since hydrates need water molecules to grow, it is expected that the growth is faster in the aqueous phase.

### 3.2. Simulations of the Unconstrained Hydrate Seeds

Under the same conditions as we used for the runs presented in the previous section—400 bar and 255 K—we carried out simulations in which the positions of the seeds inserted into the system were not constrained. This time seeds of different sizes were used, with a radius ranging from 1.3 to 2.0 nm. The starting configurations for these runs were equilibrated as described in Supporting Information, where we show that the specific protocol used for the equilibration of the seed interface does not affect the results.

An example of the evolution of the seeds after 40 ns is shown in Figure 5. As can be seen, the seeds originally inserted into the system close to, or immersed in, the $CO_2$-rich phase tend to drift away from the interface into the aqueous solution. This observation clashes with the hypothesis that nucleation takes place at the interface.


https://doi.org/10.1021/acs.jpcb.5c07607
J. Phys. Chem. B XXXX, XXX, XXX−XXX

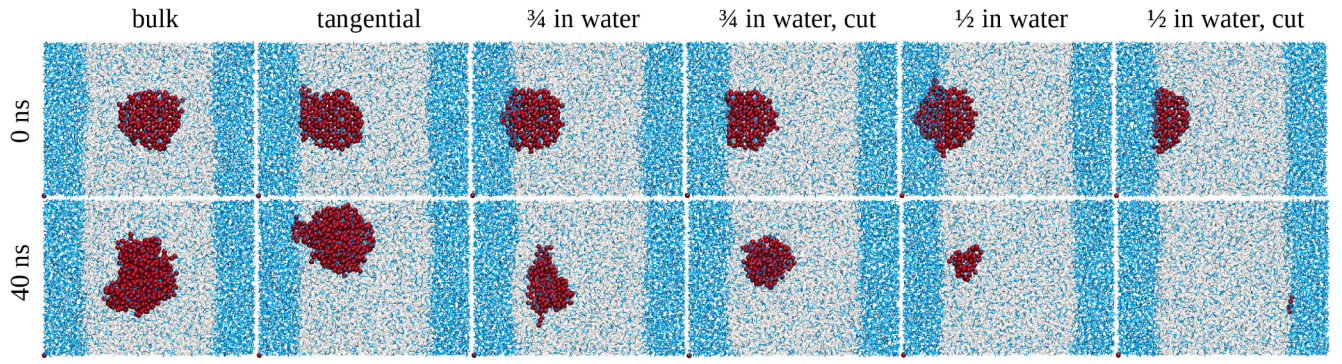


**Figure 5.** Snapshots of the system in unrestrained production runs at 0 and 40 ns. The starting radius of the seeds was 1.7 nm in all cases. The molecules of water that were found to belong to the biggest hydrate cluster (identified as in ref 55) are presented as red spheres. Water molecules in the liquid phase and $CO_2$ molecules are shown as gray and cyan lines, respectively. The graphic was created using VMD[69] software.

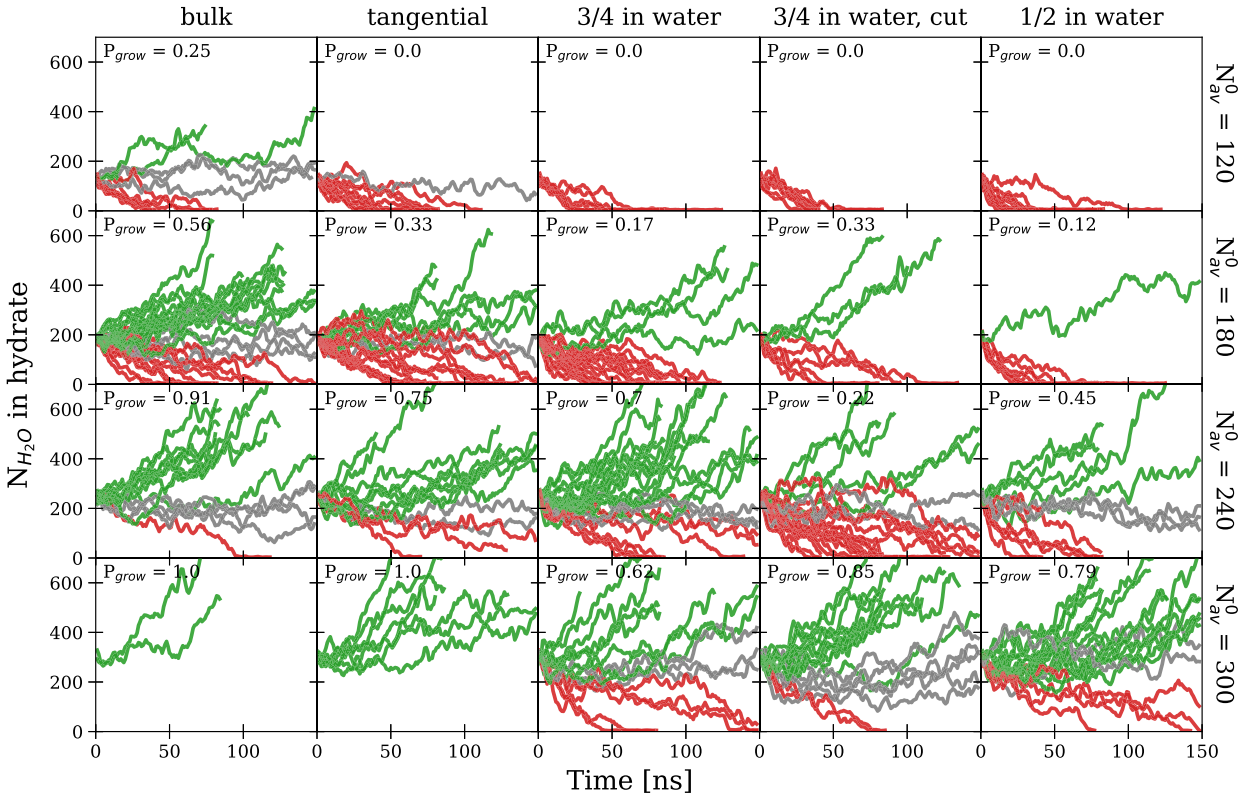


**Figure 6.** Changes in time of the size of the hydrate seed during production runs. Results are shown in separate rows according to the average size of the seed in the first 3 ns of a given production run. The average sizes of the seeds at the start of the runs presented within each row are indicated on the right-hand side of the figure. In the figure, the data for only a few starting seed sizes is shown (an extended figure with all initial sizes considered is presented in Supporting Information). The different seed locations/shapes are organized in different columns. Lines in the figure are colored in red if the seed melts and in green if it grows, while gray lines are used for the runs in which the size of the seed is stable (not changing enough to label it as either "growing" or "melting"). The probability of growing was calculated in each plot based on the number of growing and melting seeds (the runs labeled as "stable" were not included in the calculations).

Depending on the location, shape and size of the seed at the beginning of the trajectory, the outcomes we observed were different. In some cases, the seeds were growing in most of the runs, in others they were almost always melting. To organize all these results, we analyzed changes in time of the seed sizes. The results are presented in Figure 6.

In the figure, the different seed locations are organized in columns, while rows correspond to a similar size of the seeds at the beginning of the trajectory (within a range of 20 water molecules around the average value shown on the right side of the figure). For clarity, only a few starting sizes of the seeds are included in Figure 6 (see Figure S2 in Supporting Information for the figure including all runs). The *1/2 in water, cut* type was not included in the figure, since in the majority of the runs, regardless of the starting seed size, the seeds were melting. Trajectories are colored in green and red if the seed size either increases or decreases significantly during the run (the change of the size must be greater than 50% compared to the starting size of the seed). Trajectories are colored in gray if the change of the seed size was smaller than 50%. The growth probability indicated inside each plot corresponds to the ratio between the number of green trajectories and the sum of green and red


https://doi.org/10.1021/acs.jpcb.5c07607
J. Phys. Chem. B XXXX, XXX, XXX−XXX

ones (gray ones are not considered for calculating the probability).

The growth probability increases as one moves down a given column. This trend is expected, since the size of the seed from which the trajectories are initiated increases down the column (the larger the seed is, the more likely it is that it grows).

By examining a particular row in Figure 6, one can clearly observe that the probability of growth decreases from left to right, as the seed is placed closer to the interface. The finding that the interface hinders the growth of hydrate seeds is one of the main results of this work.

As mentioned before, within each panel in Figure 6, we report the corresponding probability of growth. These probabilities are then plotted in Figure 7 as a function of the initial seed size for all seed locations and shapes considered. Although the curves are somewhat noisy due to limited statistics, one can clearly see that the cyan curve—corresponding to *bulk* spherical clusters—stands above the others, indicating that spherical clusters embedded in the bulk molecular environment have the highest tendency to grow. In contrast, the curves corresponding to the *1/2 in water* and *3/4 in water, cut* configurations (green and purple, respectively) fall below the rest, revealing that these locations are highly unfavorable. The *1/2 in water, cut* cluster type is even less favorable, but it does not appear in the figure because the growth probability was close to zero for all studied seed sizes. Overall, the results clearly demonstrate that clusters have a reduced chance of growing when placed near or at the interface.

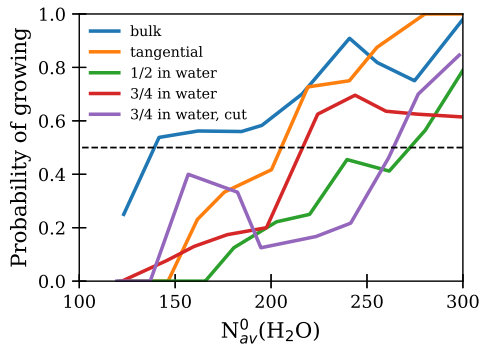


**Figure 7.** Probability of growing of hydrate seeds as a function of the initial seed size (measured as the number of water molecules belonging to the seed) for different system types (see legend).

Furthermore, truncating a cluster so that it presents a planar facet at the reservoir-solution interface does not promote growth. This becomes most evident when comparing the *1/2 in water* and *1/2 in water, cut* shapes: whereas clusters in the latter configuration (a hemisphere) never grew, spherical seeds reached a 50% growth probability for sizes larger than about 250 water molecules (see green curve in Figure 7). The observation that planar faces are disfavored is consistent with Figure 3, where we show that clusters spontaneously adopt a rounded shape as they grow. We emphasize that the comparison in Figure 7 is made at fixed numbers of water molecules in the seed. Had the comparison instead been carried out at fixed radius, truncated clusters would have had an even lower probability of growth, since they contain fewer molecules than their spherical counterparts (for a fixed radius).

### 3.3. Estimation of the Nucleation Rate for Different Seed Types

Based on Figure 7 it is possible to estimate the critical size of the seed types considered in this work. The horizontal dashed line in Figure 7 corresponds to a 50% probability. We identify the critical size, $N_c$, as that for which the growth probability is 50% (the crossing between the horizontal dashed line and a given colored line). The smaller the critical cluster is, the higher the nucleation probability of a certain seed type. The estimated critical cluster sizes for most of the seed types examined in this study are reported in Table 1 (for the *1/2 in water, cut* configuration almost all clusters melted and no critical size could be determined, so we presume it is larger than the rest). From smallest to largest $N_c$ the investigated seed types can be sorted as follows: *bulk*; *tangential*; *3/4 in water*; *3/4 in water, cut*; *1/2 in water*; *1/2 in water, cut*. This sequence confirms that bulk (homogeneous) nucleation is more favored than nucleation near or at the interface. Furthermore, it indicates that, at the conditions under study, spherical clusters

**Table 1. Nucleation Rate of $CO_2$ Hydrate in Water, $J$, Obtained from the Seeding Simulations at 255 K, 400 Bar, for Different System Types, and Parameters Used in Order to Obtain Nucleation Rates**[abcd]

| | Bulk | Tangential | 3/4 in water | 3/4 in water, cut | 1/2 in water |
|---|---|---|---|---|---|
| $N_c^{H_2O}$ | 140 | 205 | 217 | 264 | 272 |
| $N_c^{CO_2}$ | 24.3 | 35.7 | 37.7 | 45.9 | 47.3 |
| $\Delta G_c/(k_BT)$ | 27.5 | 40.3 | 42.6 | 51.9 | 53.5 |
| $J$ ($m^{-3}$ $s^{-1}$) | $1 \times 10^{23}$ | $4 \times 10^{17}$ | $4 \times 10^{16}$ | $4 \times 10^{12}$ | $8 \times 10^{11}$ |
| Parameters used for calculation of $J$ | | | | | |
| $Z$ | | | | 0.08 | |
| $f^+_{CO_2}$ ($s^{-1}$) | | | | $6.54 \times 10^8$ | |
| $\rho_L^{CO_2}$ ($m^{-3}$) | | | | $2.6 \times 10^{27}$ | |

[a]The size of the critical cluster was estimated as number of water molecules belonging to the hydrate, with the use of linear combination of $\bar{q}_3$ and $\bar{q}_{12}$ order parameters.[55] [b]The number of $CO_2$ molecules in the critical cluster was then calculated by dividing $N_c^{H_2O}$ by a factor of 5.75, which corresponds to the water to $CO_2$ ratio in a crystalline sI hydrate. [c]Note that $N_c^{CO_2}$ is equivalent to the number of cages given that we cut the seeds from a thermalised, fully occupied $CO_2$ hydrate lattice. [d]The estimated uncertainty for the critical nucleus size is ±20 water molecules (estimated from the bin width used to classify initial seed sizes), leading to relative uncertainties of about 5−10% in the nucleation barrier and to nucleation rate uncertainties ofapproximately 4−5 orders of magnitude.


https://doi.org/10.1021/acs.jpcb.5c07607
J. Phys. Chem. B XXXX, XXX, XXX−XXX

are preferred to truncated ones (with the flat face lying on the reservoir-solution interface).

Knowing $\Delta\mu_N$, the chemical potential difference between the crystal and the solution (which we calculated in our previous work for the same conditions, 255 K and 400 bar,[61] and is equal to −2.26 $k_BT$), we can then calculate the free energy barrier for nucleation, $\Delta G_c$, using the Classical Nucleation Theory[70−73] result: $\Delta G_c = |\Delta\mu_N|N_c/2$. It is then possible to go further and estimate the nucleation rate using

$$J = \rho_L^{CO_2} Z f_{CO_2}^{+} \exp\left(\frac{-N_c^{CO_2}|\Delta\mu_N|}{2k_BT}\right) \quad (1)$$

where $\rho_L^{CO_2}$ is the number density of $CO_2$ in the liquid phase, $N_c^{CO_2}$ is the number of molecules of $CO_2$ in the critical cluster, $Z$ is the Zeldovich factor and $f_{CO_2}^{+}$ is the attachment rate.

In order to estimate nucleation rates in our systems, we used the same values of $Z$ and $f_{CO_2}^{+}$ as in our previous work.[55] $\rho_L^{CO_2}$ is simply the number density of $CO_2$ in the aqueous phase. The parameters used for the calculation of the nucleation rate, as well as the nucleation rate itself, are reported in Table 1. Note that the value we obtain for nucleation of *bulk* seeds ($J = 10^{23}$ m$^{-3}$ s$^{-1}$) is consistent within 2 orders of magnitude with the value we published in ref 55 of $J = 10^{25}$ m$^{-3}$ s$^{-1}$ (4−5 orders of magnitude is a typical error bar of Seeding nucleation rate calculations).[74,75]

These estimates, although rough, illustrate that the nucleation rate decreases by many orders of magnitude from a nucleus emerged in the bulk molecular environment to other less favorable locations close to or immersed in the $CO_2$-rich phase. Even the nucleation in the second-best seed type, *tangential*, is about 6 orders of magnitude slower than bulk nucleation. When a spherical nucleus is placed with its equatorial line at the interface (*1/2 in water* location) one obtains nucleation rates more than 10 orders of magnitude slower than in the bulk. We do not find, therefore, any evidence of a preferred nucleation at the interface in our seeding simulations.

Let us revisit, however, the spontaneous nucleation simulations we performed in our previous work[55] at lower temperatures (245 and 250 K) to check whether this finding is affected by the artificial Seeding of the hydrates cluster in the system.

### 3.4. Unseeded Spontaneous Nucleation

In previous work,[55] we demonstrated that at 245 and 250 K under the pressure of 400 bar, spontaneous hydrate nucleation occurs within hundreds of nanoseconds. Furthermore, we found that the nucleation time is identical in a $CO_2$-saturated bulk aqueous solution and in a two-phase system, where a slab of the aqueous solution is saturated with $CO_2$ by contact with a reservoir through a flat interface (note that the $CO_2$ concentration in the aqueous phase is the same in one-phase and two phase-systems). This finding clearly shows that, at least at these two temperatures, the presence of the interface does not accelerate nucleation. Moreover, this result also remarks that bulk-like behavior can be found in the aqueous slab of the two-phase system, as illustrated by the density profiles shown in Figure 2.

To corroborate this result, we analyze in this work the location of hydrate nuclei that appear spontaneously at 250 K in the two-phase system. According to the Seeding analysis performed in this work and to the spontaneous nucleation rate calculations conducted in ref 55, it is expected that these nuclei do not appear at the interface. In Figure 8 we show the center of mass location of the nucleus along time using a certain color code depending on the nucleus size (see legend) and for a selected spontaneous nucleation trajectory at 250 K. The horizontal dashed lines indicate the average location of the interface between the $CO_2$-rich and the water-rich phases. Clearly, the nucleus does not appear close to any of the two interfaces, corroborating our main result that nucleation does not take place at the interface. A similar behavior was observed in all nucleating trajectories. In ref 76, where spontaneous $CH_4$ hydrate nucleation was studied in systems containing a $CH_4$ bubble embedded in the aqueous solution, they observed the appearance of the hydrate nucleus away from the bubble-aqueous solution interface, in agreement with what we see here for planar interfaces.

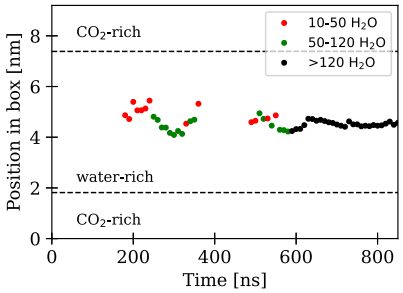


**Figure 8.** Dots indicate the coordinate perpendicular to the interface of the center of mass of the of the largest hydrate nucleus in a spontaneous nucleation trajectory at 250 K and 400 bar. The average location of the interfaces is indicated with the dashed horizontal lines. Different dot colors represent different size ranges of the nucleus (see legend), in terms of number of water molecules. Only sizes larger than 10 water molecules were considered.

In Figure 9 we show an analysis of the spontaneous nucleation path in bulk and two-phase systems. In the top part of the figure we show the number of $CO_2$ molecules in the largest hydrate cluster identified with the MCG-3 algorithm.[77] Below these plots, three snapshots of the systems at times specified by colored dots are presented.

For this particular analysis we chose the MCG-3 order parameter because it allows to identify the molecules of $CO_2$ belonging to the hydrate seed, unlike the linear combination of $\bar{q}_3$ and $\bar{q}_{12}$ order parameters[55] used in Table 1 which refers to water molecules. The MCG-3 order parameter labels a molecule of $CO_2$ as hydrate if a set of geometrical criteria is met. First, a molecule of $CO_2$ has to have a neighboring molecule of $CO_2$ within 9 Å and this pair of $CO_2$ molecules has to have at least 5 molecules of water "shared" between them. "Shared" water molecules, as described in ref 77, correspond to molecules of water inside an area limited by two cones located along the line connecting the two $CO_2$ molecules and starting in the carbon atoms of $CO_2$ molecules (semivertical angles of the cones are equal to 45°). Second, a molecule of $CO_2$ can be labeled as hydrate only if it forms at least three pairs described in the previous step.

In the snapshots of Figure 9, molecules of $CO_2$ labeled as hydrate by the MCG-3 order parameter and the molecules of water "shared" by pairs of $CO_2$ molecules in the hydrate are highlighted in orange and red, respectively. Additionally, we searched for regions in the system where the concentration of


https://doi.org/10.1021/acs.jpcb.5c07607
J. Phys. Chem. B XXXX, XXX, XXX−XXX

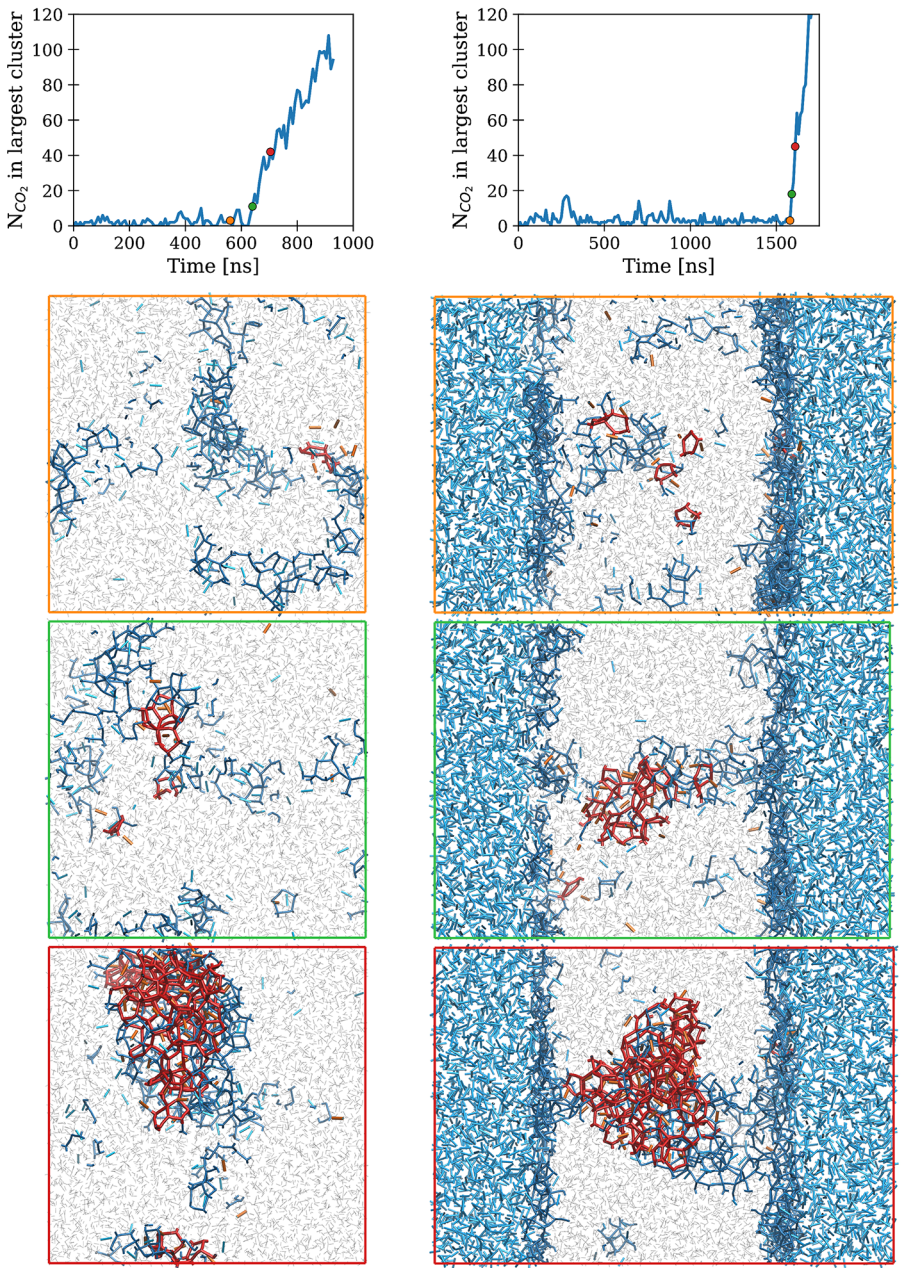


**Figure 9.** Top panel: size of the largest hydrate cluster in time in representative spontaneous nucleation trajectories in the one-phase and the two-phase systems at 400 bar and 250 K. For three moments in each trajectory, indicated by colored dots in the top plots, snapshots framed in the corresponding color are shown below. The clusters of hydrate recognized by the MCG-3 order parameter are marked with orange ($CO_2$ molecules) and red (water molecules) bonds. Areas of locally higher density of $CO_2$ are also shown, as light blue ($CO_2$ molecules) and dark blue (water molecules) bonds. The areas of high $CO_2$ density were found by looking for molecules of $CO_2$ that have 11 or more neighboring molecules of $CO_2$ (within distance of 0.9 nm). The graphic was created using VMD[69] software.

$CO_2$ was locally higher than the average. For that purpose, we found molecules of $CO_2$ that have at least 11 neighboring $CO_2$ molecules within 9 Å (the same distance criterion as for the MCG-3 order parameter) and highlighted them in cyan. For each pair of $CO_2$ molecules found this way, we also highlighted (in dark blue) the molecules of water "shared" between them.

It is worth noting that MCG-3 does not label molecules of water as either hydrate or liquid. However, it enables identification of regions with a high local $CO_2$ concentration and $CO_2$ molecules in a hydrate-like arrangement. Thus, it is a suitable order parameter for our purpose of studying from a qualitative perspective the emergence of hydrates in regions of locally high $CO_2$ concentration. For obtaining quantitative estimates of the nucleation rate (Section 3.3) we chose the linear combination of $\overline{q}_3$ and $\overline{q}_{12}$ proposed in ref 55, which was previously shown to provide seeding estimates of $J$ in good agreement with spontaneous nucleation.[55]

As can be seen in the top part of Figure 9, in both system types - bulk and containing planar interface with a $CO_2$ reservoir - there is an induction period of a few hundreds of nanoseconds where small clusters of hydrate form and redissolve until a stochastic fluctuation gives rise to a critical cluster that quickly grows.


https://doi.org/10.1021/acs.jpcb.5c07607
J. Phys. Chem. B XXXX, XXX, XXX−XXX

In the snapshots we can see a similar nucleation mechanism in both cases. The presence of cyan-blue clustered regions before nucleation indicates that there is strong $CO_2$ density heterogeneities. Obviously, in the two-phase system the interface corresponds to one of these regions, but there are also clear $CO_2$ density fluctuations in the bulk aqueous phase. Interestingly, hydrate clusters always appear within a bulk high $CO_2$ density regions. Thus, we envisage a mechanism where $CO_2$ density fluctuations facilitate the emergence of hydrate clusters (in fact, spontaneous $CH_4$ nucleation occurs when the solution is supersaturated with methane).[27] Similar observation of nucleation in regions of high local guest molecule concentration has already been reported in previous works.[56,57,78] However, our analysis reveals that these fluctuations are present both close to the $CO_2$-aqueous solution interface and in the bulk aqueous phase, but the proximity of the interface disrupts the nucleation of the hydrate, making the bulk aqueous solution the preferred location for nucleation.

## 4. DISCUSSION

Our simulations clearly show that nucleation preferentially occurs in the bulk. Does our work imply that hydrate nucleation also takes place in the bulk in real systems? Experiments observe hydrate appearance and growth at the interface.[16,18−21] Here we provide some speculative hypotheses to reconcile our simulation results with experimental observations.

One possibility is that nucleation takes place in the bulk (homogeneous nucleation) and then the nucleus attaches to the interface, where it subsequently grows. However, this scenario seems unlikely because experiments generally observe hydrate nucleation at temperatures a few kelvin below the dissociation temperature,[13,14,18−20,79] and several simulation studies estimate that homogeneous nucleation is not possible at such a small supercooling.[31,55]

Where, then, is nucleation actually taking place? One possibility is that there is a crossover from bulk (homogeneous) to interfacial (heterogeneous) nucleation as temperature increases. In our simulations, bulk nucleation of $CO_2$ hydrates is faster at 245, 250, and 255 K. However, the homogeneous nucleation rate drops rapidly with increasing temperature. In contrast, the interfacial nucleation rate may have a weaker temperature dependence. This opens the possibility that at higher temperatures interfacial nucleation becomes dominant.

Another plausible scenario is that nucleation happens in the contact line between the aqueous solution, the hydrate-former rich phase and the cell walls. This possibility has been proposed in several papers[14,16,17,20] and may also explain why higher supercoolings are typically observed when hydrate formation occurs in droplets suspended without contact with solid walls.[16,20,80] Additionally, the presence of impurities, both in the bulk or trapped at the interface, may also increase the temperature at which hydrate formation is observed. Simulations show that solid surfaces can indeed promote hydrate nucleation.[58,81]

We emphasize that our work focuses on the early nucleation stage. Rapid growth may require a fast supply of hydrate-former molecules - $CO_2$ in our case - from the hydrate-former-rich phase. Consequently, nucleation and early growth may occur in the bulk molecular environment (homogeneous nucleation), whereas sustained growth may require the postcritical nucleus to be in close proximity to the interface. The time and length scales required to investigate such growth processes are beyond those accessible to our molecular simulations.

Our work appears to clash with a recent simulation study where nucleation is reported to take place at the interface at high supercooling.[58] A possible difference between our work and that of ref 58 is that they use $H_2S$ instead of $CO_2$ as hydrate former. For the model used in this work for $CO_2$ the solubility of $CO_2$ decreases as the temperature increases,[55] whereas in ref 58 the solubility of $H_2S$ increases as $T$ increases (see Figure 4d in ref 58). Experimentally the solubility of both guest molecules decreases as T increases, at least under low pressures.[82] Further studies are needed to clarify whether there are fundamental differences between $H_2S$ and $CO_2$ hydrate nucleation.

In any case, our results challenge the commonly held view that hydrate nucleation universally occurs at interfaces. At high supercooling, bulk (homogeneous) nucleation may in fact dominate. More work is needed to understand the nucleation mechanism at moderate supercooling, where most experimental observations are made.

A promising direction is the direct comparison of nucleation rates from simulations and experiments. This quantity provides a natural bridge between both approaches, allowing validation of simulations, which offer access to molecular-level details that are often inaccessible experimentally. For ice nucleation, the nucleation rate has already been successfully compared between simulations (using the same water model as in the present work) and experiments[75,83] (even though there is still an open debate over the competition between bulk and surface ice nucleation in small water drops).[84,85] Unfortunately, for hydrates, very few experimental measurements of nucleation rates are available. In contrast, there are already several simulation studies where hydrate nucleation rates have been calculated. Most of them focus on the bulk, but often using aqueous solutions with unrealistically high hydrate-former concentrations.[29,31,54,55,86]

Our simulations suggest that at sufficiently high supercooling, homogeneous (bulk) nucleation should outpace interfacial nucleation. This regime may offer a valuable opportunity to directly measure homogeneous nucleation rates and compare them with existing simulation predictions, thereby laying a stronger foundation for the molecular-level understanding of hydrate nucleation.

## 5. SUMMARY AND CONCLUSIONS

We employ molecular dynamics simulations of a realistic water−$CO_2$ model to examine the formation of $CO_2$ hydrates in supercooled, $CO_2$-saturated aqueous solutions at 400 bar. Most simulations are carried out at 255 K, corresponding to a supercooling of 35 K below the hydrate−solution−$CO_2$ triple point.[61] Hydrate seeds are introduced at different positions relative to the interface to monitor their growth. Interestingly, we find that hydrate nucleation proceeds more rapidly in the bulk than near the interface, challenging the conventional view. We also explore spontaneous nucleation pathways (without seeding) at 250 K, a higher supercooling that enables homogeneous hydrate nucleation within our simulation time scale. In this regime, nucleation occurs preferentially in regions with locally enhanced $CO_2$ concentration due to thermal fluctuations; these regions arise in the bulk and are not associated with the interface. Our findings highlight the need


https://doi.org/10.1021/acs.jpcb.5c07607
J. Phys. Chem. B XXXX, XXX, XXX−XXX

for careful investigation of hydrate nucleation mechanisms, a process of critical relevance to flow assurance in the oil industry and to natural environmental systems. Further work is required to reconcile these observations with experimental evidence on hydrate nucleation and growth.

## ■ ASSOCIATED CONTENT

### Supporting Information

The Supporting Information is available free of charge at https://pubs.acs.org/doi/10.1021/acs.jpcb.5c07607.

Additional details on the equilibration protocol used in this study; an extended version of Figure 6 showing hydrate size evolution across all simulations (PDF)

## ■ AUTHOR INFORMATION


### Corresponding Authors

**Joanna Grabowska** − *Department of Physical Chemistry, Faculty of Chemistry, Gdansk University of Technology, Gdansk 80-233, Poland;* orcid.org/0000-0002-1074-763X; Email: joanna.grabowska@pg.edu.pl

**Eduardo Sanz** − *Dpto. Química Física I, Fac. Ciencias Químicas, Universidad Complutense de Madrid, Madrid 28040, Spain;* orcid.org/0000-0001-6474-5835; Email: esa01@quim.ucm.es

### Authors

**Samuel Blazquez** − *Dpto. Química Física I, Fac. Ciencias Químicas, Universidad Complutense de Madrid, Madrid 28040, Spain;* orcid.org/0000-0002-6218-3880

**Carlos Vega** − *Dpto. Química Física I, Fac. Ciencias Químicas, Universidad Complutense de Madrid, Madrid 28040, Spain;* orcid.org/0000-0002-2417-9645

Complete contact information is available at: https://pubs.acs.org/10.1021/acs.jpcb.5c07607


### Notes

The authors declare no competing financial interest.

## ■ ACKNOWLEDGMENTS

J.G. gratefully acknowledges the Polish high-performance computing infrastructure PLGrid (HPC Center: ACK Cyfronet AGH) for providing computer facilities and support within computational grant no. PLG/2025/018076. Computations were carried out using the computers of the Centre of Informatics, Tricity Academic Supercomputer & Network. C.V., E.S., and S.B. acknowledge funding from project PID2022-136919NB-C31 of the Ministerio de Ciencia, Innovación y Universidades.

## ■ REFERENCES


(1) Sloan, E. D.; Koh, C. *Clathrate Hydrates of Natural Gases*. 3rd ed.; CRC Press: New York, 2008.

(2) Hirohama, S.; Shimoyama, Y.; Wakabayashi, A.; Tatsuta, S.; Nishida, N. Conversion of ch4-hydrate to co2-hydrate in liquid co2. *J. Chem. Eng. Jpn* **1996**, *29*, 1014−1020.

(3) Park, Y.; Kim, D.-Y.; Lee, J.-W.; Huh, D.-G.; Park, K.-P.; Lee, J.; Lee, H. Sequestering carbon dioxide into complex structures of naturally occurring gas hydrates. *Proc. Natl. Acad. Sci. U. S. A* **2006**, *103*, 12690−12694.

(4) Lee, H.; Seo, Y.; Seo, Y.-T.; Moudrakovski, I. L.; Ripmeester, J. A. Recovering methane from solid methane hydrate with carbon dioxide. *Angew. Chem., Int. Ed* **2003**, *42*, 5048−5051.

(5) Lee, S.; Lee, Y.; Lee, J.; Lee, H.; Seo, Y. Experimental verification of methane−carbon dioxide replacement in natural gas hydrates using a differential scanning calorimeter. *Environ. Sci. Technol* **2013**, *47*, 13184−13190.

(6) Sloan, E. D. Hydrocarbon hydrate flow assurance history as a guide to a conceptual model. *Molecules* **2021**, *26*, 4476.

(7) Lekvam, K.; Ruoff, P. A reaction kinetic mechanism for methane hydrate formation in liquid water. *J. Am. Chem. Soc* **1993**, *115*, 8565−8569.

(8) Devarakonda, S.; Groysman, A.; Myerson, A. S. THF−water hydrate crystallization: an experimental investigation. *J. Cryst. Growth* **1999**, *204*, 525.

(9) Takeya, S.; Hori, A.; Hondoh, T.; Uchida, T. Freezing-memory effect of water on nucleation of $CO_2$ hydrate crystals. *J. Phys. Chem. B* **2000**, *104*, 4164.

(10) Herri, J. M.; Pic, J. S.; Gruy, F.; Cournil, M. Methane hydrate crystal- lization mechanism from in-situ particle sizing. *AIChE J* **1999**, *45*, 590.

(11) Abay, H. K.; Svartaas, T. M. Multicomponent gas hydrate nucleation: The effect of the cooling rate and composition. *Energy Fuels* **2011**, *25*, 42.

(12) Jensen, L.; Thomsen, K.; von Solms, N. Propane hydrate nucleation: Experimental investigation and correlation. *Chem. Eng. Sci* **2008**, *63*, 3069−3080.

(13) Maeda, N. Nucleation curves of methane hydrate from constant cooling ramp methods. *Fuel* **2018**, *223*, 286.

(14) Maeda, N.; Shen, X. D. Scaling laws for nucleation rates of gas hydrate. *Fuel* **2019**, *253*, 1597.

(15) Liang, R.; Xu, H.; Shen, Y.; Sun, S.; Xu, J.; Meng, S.; Shen, Y. R.; Tian, C. Nucleation and dissociation of methane clathrate embryo at the gas−water interface. *Proc. Natl. Acad. Sci. U. S. A* **2019**, *116*, 23410−23415.

(16) Maeda, N. Nucleation curves of model natural gas hydrates on a quasi-free water droplet. *AIChE J* **2015**, *61*, 2611−2617.

(17) Stoporev, A. S.; Semenov, A. P.; Medvedev, V. I.; Sizikov, A. A.; Gushchin, P. A.; Vinokurov, V. A.; Manakov, A. Y. Visual observation of gas hydrates nucleation and growth at a water−organic liquid interface. *J. Cryst. Growth* **2018**, *485*, 54−68.

(18) Adamova, T. P.; Stoporev, A. S.; Manakov, A. Y. Visual studies of methane hydrate formation on the water−oil boundaries. *Cryst. Growth Des* **2018**, *18*, 6713−6722.

(19) Li, C.; Metaxas, P. J.; Barwood, M. T.; Johns, M. L.; Aman, Z. M.; May, E. F. Dependence of gas hydrate formation kinetics on system size from lag time experiments in a stirred pipe. *Energy Fuels* **2025**, *39*, 1060−1069.

(20) Jeong, K.; Metaxas, P. J.; Helberg, A.; Johns, M. L.; Aman, Z. M.; May, E. F. Gas hydrate nucleation in acoustically levitated water droplets. *Chem. Eng. J* **2022**, *433*, 133494.

(21) Sloan, E. D., Jr.; Koh, C. A. *Clathrate hydrates of natural gases*. CRC press: 2007.

(22) Kashchiev, D.; Firoozabadi, A. Nucleation of gas hydrates. *J. Cryst. Growth* **2002**, *243*, 476−489.

(23) Báez, L. A.; Clancy, P. Computer simulation of the crystal growth and dissolution of natural gas hydrates. *Ann. N.Y. Acad. Sci* **1994**, *715*, 177.

(24) Rodger, P. M.; Forester, T. R.; Smith, W. Simulations of the methane hydrate/methane gas interface near hydrate forming conditions. *Fluid Phase Equilib* **1996**, *116*, 326.

(25) Alavi, S.; Ripmeester, J. A.; Klug, D. D. Molecular-dynamics study of structure II hydrogen clathrates. *J. Chem. Phys* **2005**, *123*, 024507.

(26) Alavi, S.; Ripmeester, J. A.; Klug, D. D. Molecular-dynamics simulations of binary structure II hydrogen and tetrahydrofurane clathrates. *J. Chem. Phys* **2006**, *124*, 014704.

(27) Walsh, M. R.; Koh, C. A.; Sloan, E. D.; Sum, A. K.; Wu, D. T. Microsec- ond simulations of spontaneous methane hydrate nucleation and growth. *Science* **2009**, *326*, 1095.

(28) English, N. J.; Tse, J. S. Mechanisms for thermal conduction in methane hydrate. *Phys. Rev. Lett* **2009**, *103*, 015901.

(29) Walsh, M. R.; Beckham, G. T.; Koh, C. A.; Sloan, E. D.; Wu, D. T.; Sum, A. K. Methane hydrate nucleation rates from molecular dynamics simula- tions: Effects of aqueous methane concentration, interfacial curvature, and system size. *J. Phys. Chem. C* **2011**, *115*, 21241.
(30) Sarupria, S.; Debenedetti, P. G. Homogeneous nucleation of methane hydrate in microsecond molecular dynamics simulations. *J. Phys. Chem. Lett* **2012**, *3*, 2942.
(31) Knott, B. C.; Molinero, V.; Doherty, M. F.; Peters, B. Homogeneous nucleation of methane hydrates: Unrealistic under realistic conditions. *J. Am. Chem. Soc* **2012**, *134*, 19544−19547.
(32) Liang, S.; Kusalik, P. G. Nucleation of gas hydrates within constant energy systems. *J. Phys. Chem. B* **2013**, *117*, 1403.
(33) Barnes, B. C.; Knott, B. C.; Beckham, G. T.; Wu, D.; Sum, A. K. Molecular dynamics study of carbondioxide hydrate dissociation. *J. Phys. Chem. B* **2014**, *118*, 13236−13243.
(34) Yuhara, D.; Barnes, B. C.; Suh, D.; Knott, B. C.; Beckham, G. T.; Yasuoka, K.; Wu, D.; Sum, A. K. Nucleation rate analysis of methane hydrate from molecular dynamics simualtions. *Faraday Discuss* **2015**, *179*, 463−474.
(35) Zhang, Z.; Liu, C.-J.; Walsh, M. R.; Guo, G.-J. Effects of ensembles on methane hydrate nucleation kinetics. *Phys. Chem. Chem. Phys* **2016**, *18*, 15602.
(36) Lauricella, M.; Ciccotti, G.; English, N. J.; Peters, B.; Meloni, S. Mechanisms and nucleation rate of methane hydrate by dynamical nonequilibrium molecular dynamics. *J. Phys. Chem. C* **2017**, *121*, 24223.
(37) Arjun; Berendsen, T. A.; Bolhuis, P. G. Unbiased atomistic insight in the competing nucleation mechanisms of methane hydrates. *Proc. Natl. Acad. Sci. U. S. A* **2019**, *116*, 19305.
(38) Arjun, A.; Bolhuis, P. G. Rate prediction for homogeneous nucleation of methane hydrate at moderate supersaturation using transition interface sampling. *J. Phys. Chem. B* **2020**, *124*, 8099.
(39) Arjun, A.; Bolhuis, P. G. Homogenous nucleation rate of $CO_2$ hydrates using transition interface sampling. *J. Chem. Phys* **2021**, *154*, 164507.
(40) Arjun, A.; Bolhuis, P. G. Homogeneous nucleation of crystalline methane hydrate in molecular dynamics transition paths sampled under realistic conditions. *J. Chem. Phys* **2023**, *158*, 044504.
(41) Zhang, Z.; Kusalik, P. G.; Guo, G.-J. Molecular insight into the growth of hydrogen and methane binary hydrates. *J. Phys. Chem. C* **2018**, *122*, 7771−7778.
(42) Zhang, Z.; Guo, G.-J.; Wu, N.; Kusalik, P. G. Molecular insights into guest and composition dependence of mixed hydrate nucleation. *J. Phys. Chem. C* **2020**, *124*, 25078−25086.
(43) Wang, J.-L.; Sadus, R. J. Phase Behaviour of Binary Fluid Mixtures: a Global Phase Diagram Solely in Terms of Pure Component Properties. *Fluid Phase Equilib* **2003**, *214*, 67−78.
(44) Jiménez-Ángeles, F.; Firoozabadi, A. Nucleation of methane hydrates at moderate subcooling by molecular dynamics simulations. *J. Phys. Chem. C* **2014**, *118*, 11310−11318.
(45) Jiménez-Ángeles, F.; Firoozabadi, A. Hydrophobic hydration and the effect of NaCl salt in the adsorption of hydrocarbons and surfactants on clathrate hydrates. *ACS Cent. Sci* **2018**, *4*, 820−831.
(46) Zhang, Z.-c.; Wu, N.-y.; Liu, C.-l.; Hao, X.-l.; Zhang, Y.-c.; Gao, K.; Peng, B.; Zheng, C.; Tang, W.; Guo, G.-j. Molecular simulation studies on natural gas hydrates nucleation and growth: A review. *China Geol* **2022**, *5*, 330−344.
(47) Tanaka, H.; Matsumoto, M.; Yagasaki, T. On the phase behaviors of $CH_4$−$CO_2$ binary clathrate hydrates: Two-phase and three-phase coexistences. *J. Chem. Phys* **2023**, *158*, 224502.
(48) Tanaka, H.; Matsumoto, M.; Yagasaki, T. Cage occupancies of $CH_4$, $CO_2$, and Xe hydrates: Mean field theory and grandcanonical Monte Carlo simulations. *J. Chem. Phys* **2024**, *160*, 044502.
(49) Conde, M. M.; Vega, C. Determining the three-phase coexistence line in methane hydrates using computer simulations. *J. Chem. Phys* **2010**, *133*, 064507.
(50) Míguez, J. M.; Conde, M. M.; Torré, J.-P.; Blas, F. J.; Piñeiro, M. M.; Vega, C. Molecular dynamics simulation of $CO_2$ hydrates: Prediction of three phase coexistence line. *J. Chem. Phys* **2015**, *142*, 124505.
(51) Blazquez, S.; Algaba, J.; Míguez, J. M.; Vega, C.; Blas, F. J.; Conde, M. M. Three-phase equilibria of hydrates from computer simulation. I. Finite-size effects in the methane hydrate. *J. Chem. Phys* **2024**, *160*, 164721.
(52) Algaba, J.; Blazquez, S.; Feria, E.; Míguez, J. M.; Conde, M. M.; Blas, F. J. Three-phase equilibria of hydrates from computer simulation. II. Finite-size effects in the carbon dioxide hydrate. *J. Chem. Phys* **2024**, *160*, 164722.
(53) Waage, M. H.; Vlugt, T. J. H.; Kjelstrup, S. Phase diagram of methane and carbon dioxide hydrates computed by Monte Carlo simulations. *J. Phys. Chem. B* **2017**, *121*, 7336−7350.
(54) Grabowska, J.; Blázquez, S.; Sanz, E.; Noya, E. G.; Zerón, I. M.; Algaba, J.; Míguez, J. M.; Blas, F. J.; Vega, C. Homogeneous nucleation rate of methane hydrate formation under experimental conditions from seeding simulations. *J. Chem. Phys* **2023**, *158*, 114505.
(55) Zerón, I. M.; Algaba, J.; Míguez, J. M.; Grabowska, J.; Blazquez, S.; Sanz, E.; Vega, C.; Blas, F. J. Homogeneous nucleation rate of carbon dioxide hydrate formation under experimental condition from seeding simulations. *J. Chem. Phys* **2025**, *162*, 134708.
(56) Li, L.; Zhong, J.; Yan, Y.; Zhang, J.; Xu, J.; Francisco, J. S.; Zeng, X. C. Unraveling nucleation pathway in methane clathrate formation. *Proc. Natl. Acad. Sci. U. S. A* **2020**, *117*, 24701−24708.
(57) Jacobson, L. C.; Hujo, W.; Molinero, V. Amorphous precursors in the nucleation of clathrate hydrates. *J. Am. Chem. Soc* **2010**, *132*, 11806−11811.
(58) Zhang, Z.; Kusalik, P. G.; Guo, G.-J.; Li, Y.; Huang, L.; Wu, N. Temperature-controlled gas hydrate nucleation in the heterogeneous environment. *J. Phys. Chem. Lett* **2025**, *16*, 667−674.
(59) Abascal, J. L. F.; Sanz, E.; García Fernández, R.; Vega, C. A potential model for the study of ices and amorphous water: TIP4P/Ice. *J. Chem. Phys* **2005**, *122*, 234511.
(60) Potoff, J. J.; Siepmann, J. I. Vapor-liquid equilibria of mixtures containing alkanes, carbon dioxide, and nitrogen. *AIChE J* **2001**, *47*, 1676−1682.
(61) Algaba, J.; Zerón, I. M.; Míguez, J. M.; Grabowska, J.; Blazquez, S.; Sanz, E.; Vega, C.; Blas, F. J. Solubility of carbon dioxide in water: Some useful results for hydrate nucleation. *J. Chem. Phys* **2023**, *158*, 184703.
(62) Blazquez, S.; Conde, M. M.; Vega, C. Solubility of $CO_2$ in salty water: adsorption, interfacial tension and salting out effect. *Mol. Phys* **2024**, *122*, No. e2306242.
(63) van der Spoel, D.; Lindahl, E.; Hess, B.; Groenhof, G.; Mark, A. E.; Berendsen, H. J. Gromacs: Fast, flexible, and free. *J. Comput. Chem* **2005**, *26*, 1701−1718.
(64) Hess, B.; Kutzner, C.; Van Der Spoel, D.; Lindahl, E. Gromacs 4: algorithms for highly efficient, load-balanced, and scalable molecular simulation. *J. Chem. Theory Comput* **2008**, *4*, 435−447.
(65) Nosé, S. A molecular dynamics method for simulations in the canonical ensemble. *Mol. Phys* **1984**, *52*, 255−268.
(66) Hoover, W. G. Canonical dynamics: Equilibrium phase-space distributions. *Phys. Rev. A* **1985**, *31*, 1695.
(67) Parrinello, M.; Rahman, A. Polymorphic transitions in single crystals: A new molecular dynamics method. *J. Appl. Phys* **1981**, *52*, 7182−7190.
(68) Darden, T.; York, D.; Pedersen, L. Particle mesh ewald: An n·log(n) method for ewald sums in large systems. *J. Chem. Phys* **1993**, *98*, 10089−10092.
(69) Humphrey, W.; Dalke, A.; Schulten, K. VMD − Visual Molecular Dy- namics. *J. Mol. Graphics* **1996**, *14*, 33−38.
(70) Becker, R.; Döring, W. Kinetische behandlung der keimbildung in übersättigten dämpfen. *Ann. Phys* **1935**, *416*, 719−752.
(71) Volmer, M.; Weber, A. Keimbildung in übersättigten gebilden. *Z. Phys. Chem* **1926**, *119*, 277−301.
(72) Gibbs, J. W. *On the equilibrium of heterogeneous substances*. Transactions of the Connecticut Academy of Arts and Sciences, 1876, *3*, 108−248


https://doi.org/10.1021/acs.jpcb.5c07607
J. Phys. Chem. B XXXX, XXX, XXX−XXX

(73) Gibbs, J. W. *On the equilibrium of heterogeneous substances*. Transactions of the Connecticut Academy of Arts and Sciences, 1878, *16*, 343−524
(74) Sanz, E.; Vega, C.; Espinosa, R.; Caballero-Bernal, R.; Abascal, J. L. F.; Valeriani, C. Homogeneous Ice Nucleation at Moderate Supercooling from Molecular Simulation. *J. Am. Chem. Soc* **2013**, *135*, 15008−15017.
(75) Niu, H.; Yang, Y. I.; Parrinello, M. Temperature dependence of homogeneous nucleation in ice. *Phys. Rev. Lett* **2019**, *122*, 245501.
(76) Hu, W.; Chen, C.; Sun, J.; Zhang, N.; Zhao, J.; Liu, Y.; Ling, Z.; Li, W.; Liu, W.; Song, Y. Three-body aggregation of guest molecules as a key step in methane hydrate nucleation and growth. *Commun. Chem* **2022**, *5* (1), 33.
(77) Barnes, B. C.; Beckham, G. T.; Wu, D. T.; Sum, A. K. Two-component order parameter for quantifying clathrate hydrate nucleation and growth. *J. Chem. Phys* **2014**, *140*, 164506.
(78) Vatamanu, J.; Kusalik, P. G. Observation of two-step nucleation in methane hydrates. *Phys. Chem. Chem. Phys* **2010**, *12*, 15065−15072.
(79) Metaxas, P. J.; Lim, V. W.; Booth, C.; Zhen, J.; Stanwix, P. L.; Johns, M. L.; Aman, Z. M.; Haandrikman, G.; Crosby, D.; May, E. F. Gas hydrate formation probability distributions: Induction times, rates of nucleation and growth. *Fuel* **2019**, *252*, 448−457.
(80) Davies, S. R.; Hester, K. C.; Lachance, J. W.; Koh, C. A.; Sloan, E. D. Studies of hydrate nucleation with high pressure differential scanning calorimetry. *Chem. Eng. Sci* **2009**, *64*, 370−375.
(81) Bai, D.; Chen, G.; Zhang, X.; Sum, A. K.; Wang, W. How properties of solid surfaces modulate the nucleation of gas hydrate. *Sci. Rep* **2015**, *5*, 12747.
(82) Sander, R. Compilation of henry's law constants (version 4.0) for water as solvent. *Atmos. Chem. Phys* **2015**, *15*, 4399−4981.
(83) Espinosa, J. R.; Vega, C.; Sanz, E. Homogeneous ice nucleation rate in water droplets. *J. Phys. Chem. C* **2018**, *122*, 22892−22896.
(84) Sun, G.; Tanaka, H. Surface-induced water crystallisation driven by precursors formed in negative pressure regions. *Nat. Commun* **2024**, *15*, 6083.
(85) Haji-Akbari, A.; Debenedetti, P. G. Computational investigation of surface freezing in a molecular model of water. *Proc. Natl. Acad. Sci. U. S. A* **2017**, *114*, 3316−3321.
(86) Warrier, P.; Khan, M. N.; Srivastava, V.; Maupin, C. M.; Koh, C. A. Overview: Nucleation of clathrate hydrates. *J. Chem. Phys* **2016**, *145*, 211705.




https://doi.org/10.1021/acs.jpcb.5c07607
J. Phys. Chem. B XXXX, XXX, XXX−XXX